Supporting Information

Multilevel carbon composite construction of NASICON type $NaVPO_4F$/C/CNT cathode material for enhanced-performance sodium ion batteries

Kang Tang[a], Hualing Tian[a], Yanhui Zhang[a], Yanjun Cai[a], Hong Du[a], Mofan Zhu[a], Xiang Yao[a*], Zhi Su[a,b**]

[a] College of Chemistry and Chemical Engineering, Xinjiang Key Laboratory of Energy Storage and Photoelectroctalytic Materials, Xinjiang Normal University, PR China

[b] Xinjiang University, PR China

* Corresponding author.

** Corresponding author.

E-mail addresses: yaoxiangxjnu@163.com (X. Yao), suzhixj@163.com (Z. Su).

Experimental section

Material synthesis

The $NaVPO_4F/C/CNTx$ (x=5%, 10%, 15%) was synthesized via the sol-gel method followed by high-temperature calcination. 3 mmol V_2O_5 and 1.5(1-x) g $H_2C_2O_4 \cdot 2H_2O$ were added to the beaker and stirred at 70℃ for 1 h. The mixture was then supplemented with 6 mmol NaF, 6 mmol $NH_4H_2PO_4$, and a specific quantity of CNT, followed by stirring for 5 h to yield a dark green gel. Subsequently, the gel was subjected to drying at 90℃ for 12 h. The precursor was heat-treated in a tube furnace at 350℃ in an argon atmosphere for 4 h, then the temperature was raised to 750℃ for 8 h to obtain the target product NVPF/C/CNTx (x =5%, 10%, and 15%). The preparation process of NVPF/C samples was the same as above, without adding CNT.

Material characterization

The crystal structure of the sample was characterized by X-ray diffraction (XRD, Cu Kα, Bruker D2). The microstructure of the sample was analyzed using scanning electron microscopy (SEM, Thermo Scientific Apreo 2C) and high-resolution transmission electron microscopy (HR-TEM, Talos F200S G2). The specific surface area of the material was determined by an automatic physical adsorption instrument (BET, ASAP 2020 PLUS). The carbonized sample's graphitization degree was analyzed using a Raman spectroscopy (Thermo Scientific DXR3xi). The valence states and elemental proportions were determined using X-ray photoelectron spectroscopy (XPS, Thermo Scientific K-Alpha X). The carbon content of the material is analyzed by a thermogravimetric analyzer (TG, STA-2500). The functional group composition of the sample was characterized by Fourier transform infrared spectrometer (FTIR, NICOLET iS50).

Electrochemical measurement

The manufacturing of the active pole piece is mixed by the active material, acetylene black, polyvinylidene fluoride under the mass ratio (8:1:1), dropping N-methyl pyrrolidone as a sol. After fully grinding and mixing, the slurry is evenly coated on the aluminum foil. The aluminum foil is transferred to the vacuum drying oven at 80 °C for 12 h. After being dried, it is cut into a circular pole sheet with a diameter of 12 mm, and the active material loading of the pole sheet is approximate 2.0 $mg \cdot cm^{-1}$. The CR2032 button half-cells were assembled in the glove box filled with high purity

argon gas. On the LAND Battery Test System (CT2100A), the half battery is subjected to a constant current charge and discharge test. Cyclic voltammetry (CV) curves and electrochemical impedance spectroscopy (EIS) were determined by a CHI760E electrochemical workstation. The full cell is assembled with hard carbon as anode material and NVPF/C/CNT10% as cathode material. The hard carbon was obtained by assembling a half-cell battery with sodium as the counter electrode at a current density of 30 mA g^{-1} after 3 cycles.

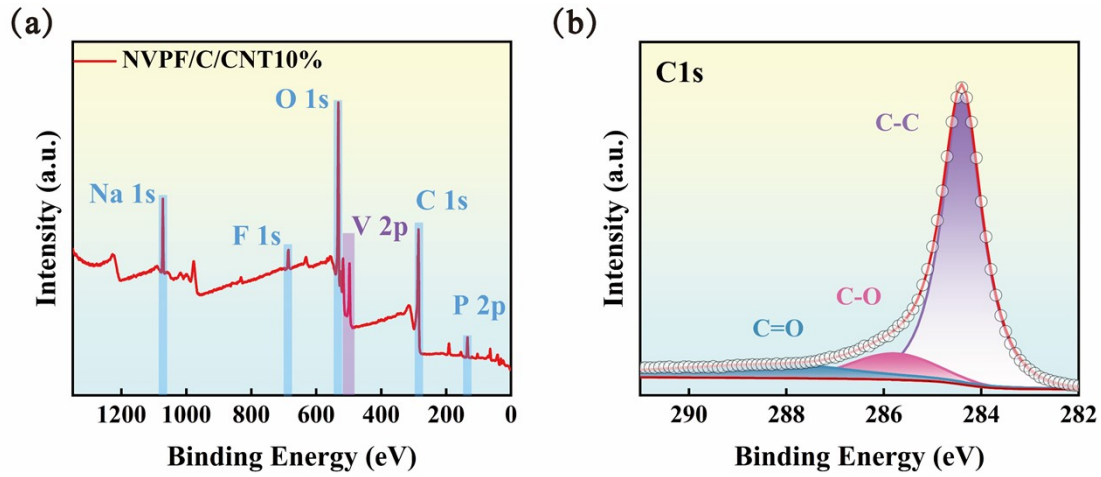

Figure S1. (a) XPS survey spectra of NVPF/C/CNT10%; (b) C 1s XPS spectra.

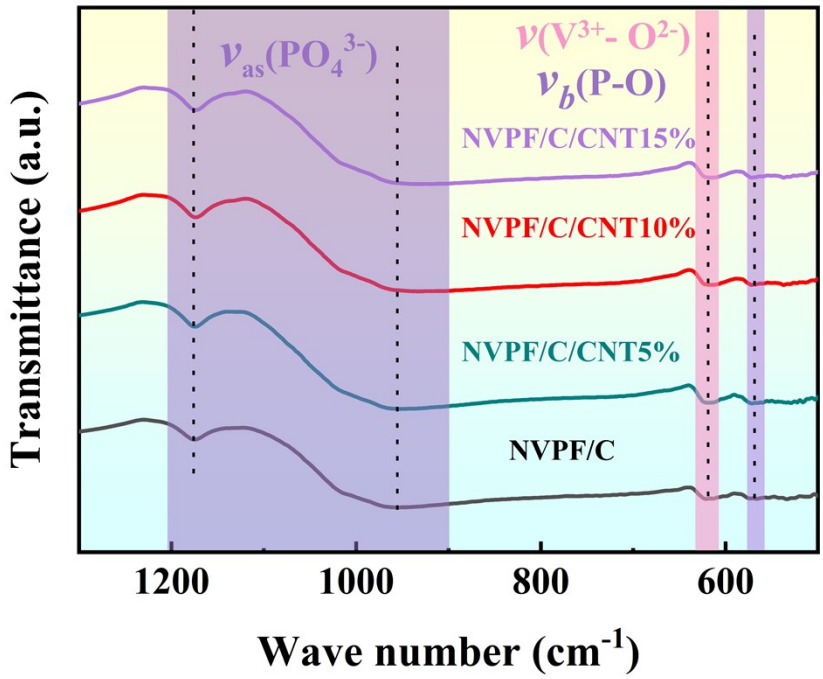

Figure S2. FTIR spectra of the four samples

FTIR spectroscopy offered critical information on the molecular structure. According to the FTIR spectra (**Figure S2**), the bands observed in the 1150~1250 cm^{-1} range can be attributed to the stretching vibrations of the PO_4 group. Furthermore, the P-O asymmetric stretching vibrations of PO_4^{3-} are clearly at 580 and 973 cm^{-1}, while the peak at 632 cm^{-1} corresponds to the V^{3+}-O^{2-} bond vibration within the VO_4F_2 octahedron. Notably, the characteristic peaks of V^{5+} (760, 950 cm^{-1}) and V^{4+} (919, 956 cm^{-1}) were absent in all four NVPF samples. This observation indicates that V^{5+} has been fully reduced to V^{3+} in all samples.

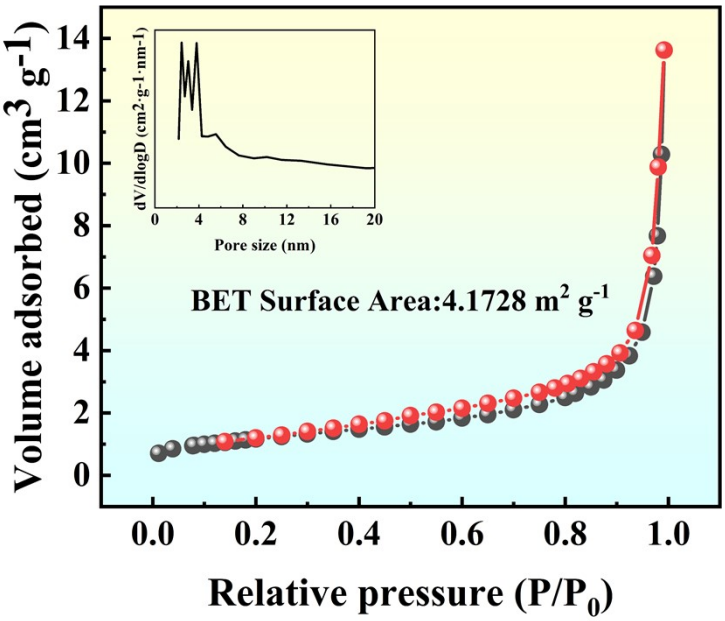

Figure S3. BET/BJH curves for NVPF/C sample.

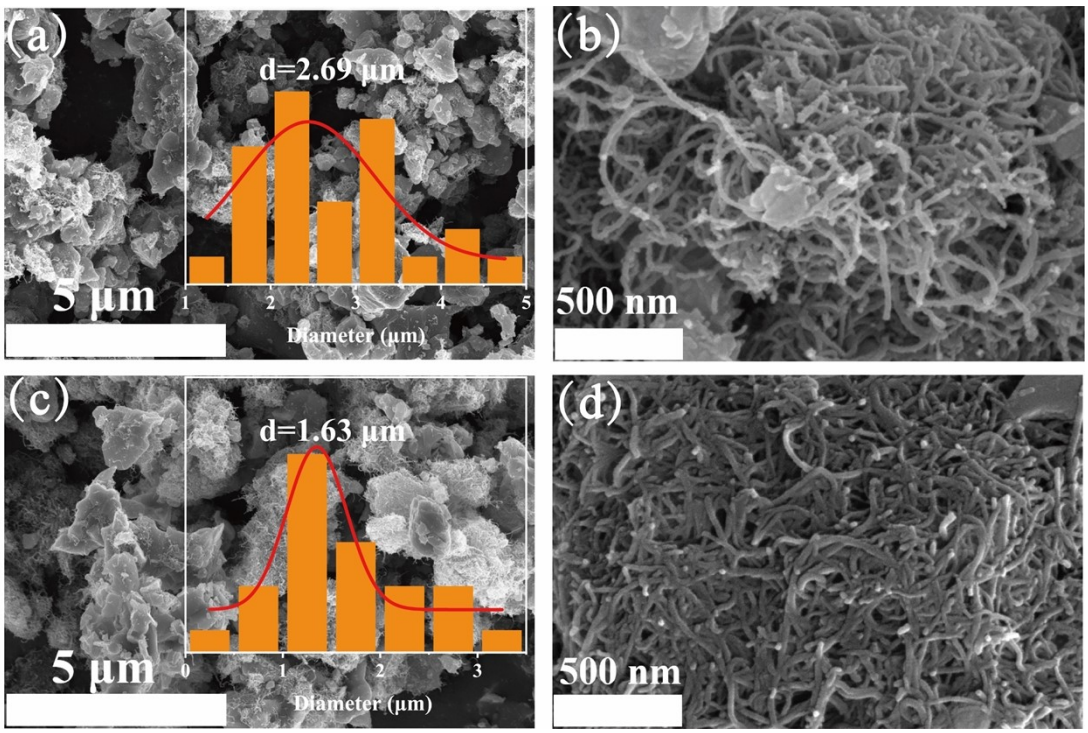

Figure S4. SEM images of (a-b) NVPF/C/CNT5%; (c-d) NVPF/C/CNT15%.

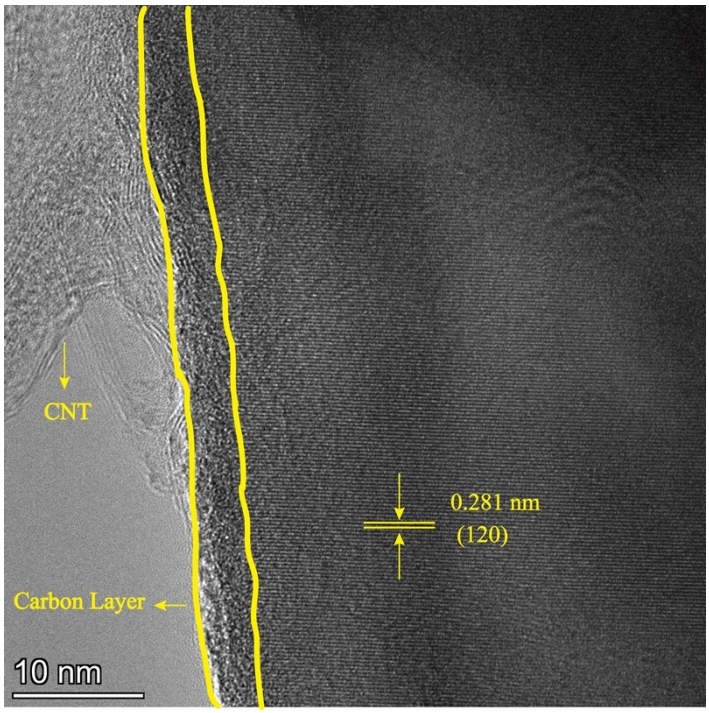

Figure S5. HRTEM images of NVPF/C/CNT10%.

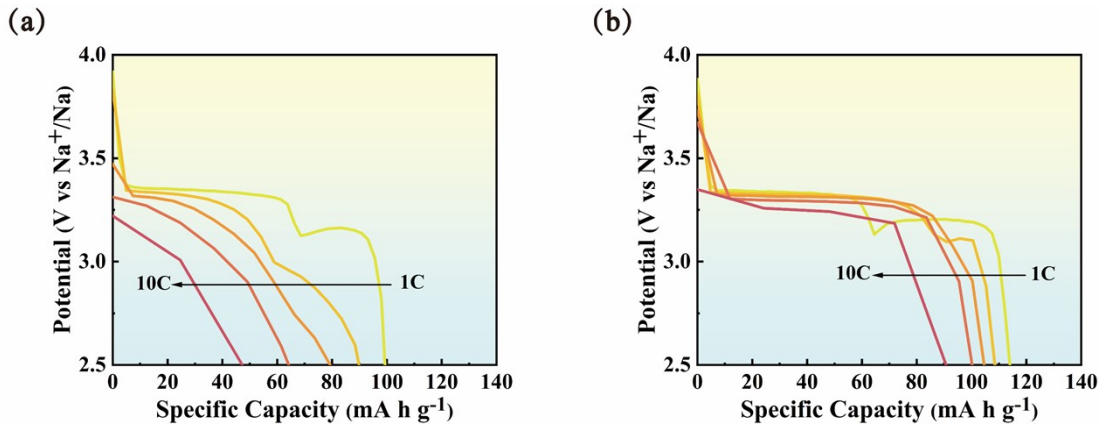

Figure S6. GCD curves of (a) NVPF/C and (b) NVPF/C/CNT10% at different rates.

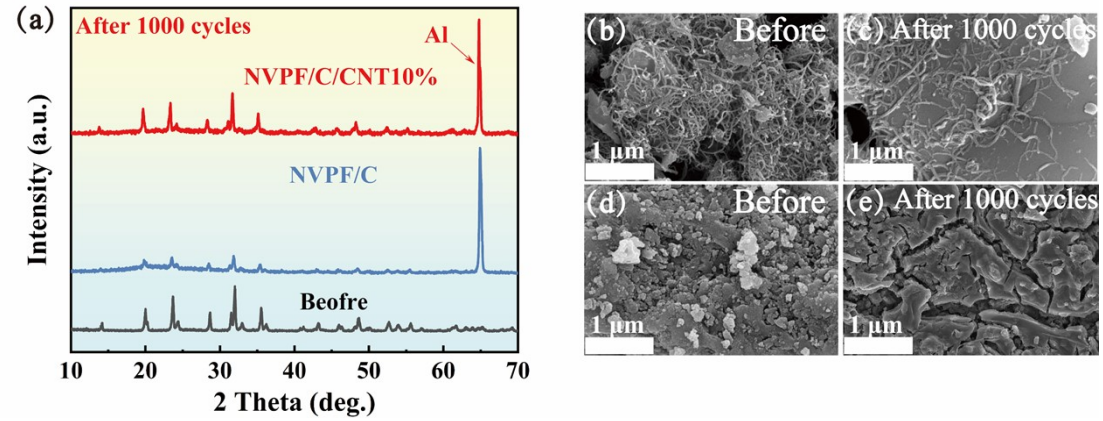

Figure S7. (a) Comparison of XRD patterns for NVPF/C and NVPF/C/CNT10% materials before and after Cycling; Comparison of SEM images before and after cycling (b-c) NVPF/C/CNT10%; (d-e) NVPF/C.

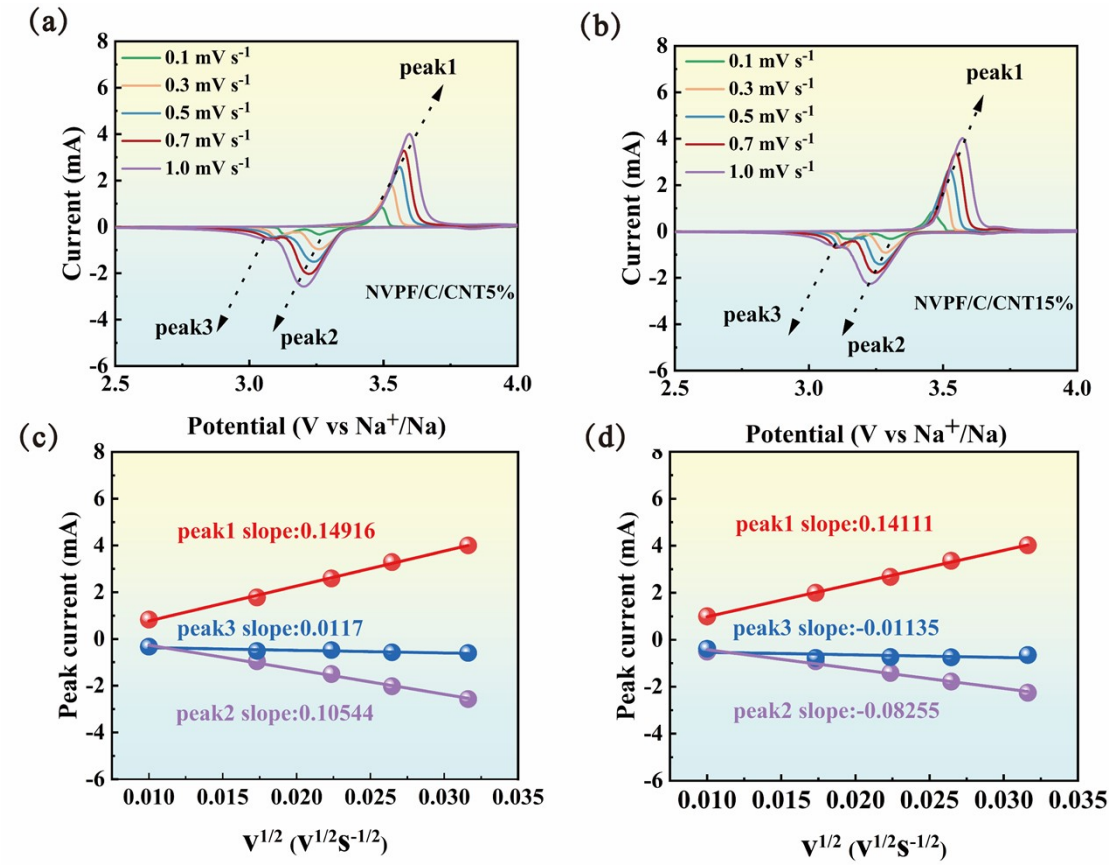

Figure S8. The CV curves obtained at various scanning rates (a) NVPF/C/CNT5%; (b) NVPF/C/CNT15%; Linear fitting graph of i_p and $v^{1/2}$ based on different sweep speeds (c) NVPF/C/CNT5%; (d) NVPF/C/CNT15%.

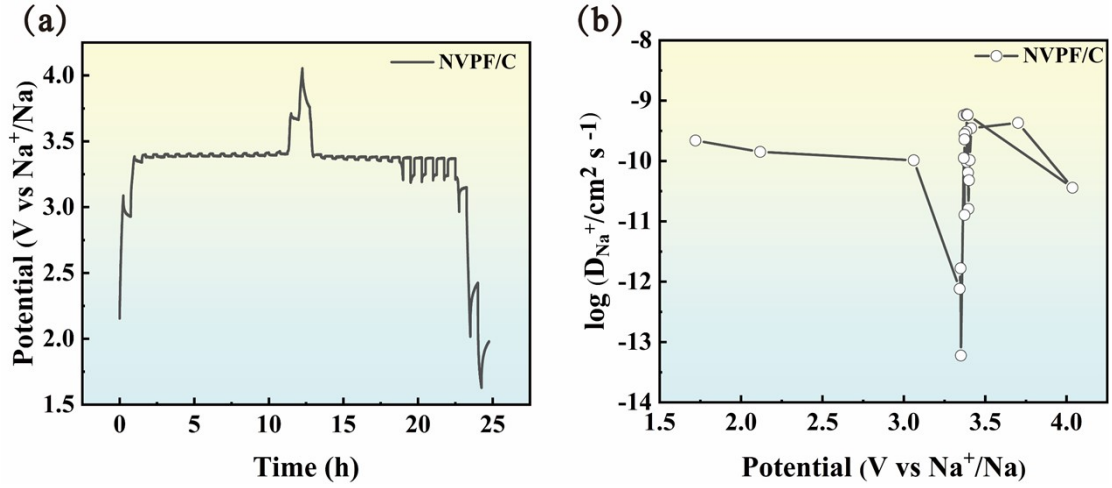

Figure S9. (a) GITT curve of NVPF/C; (b) D_{Na+} of NVPF/C .

Before measuring the GITT, the battery was charged/discharged at 0.2 C for three cycles, then charged/discharged at constant voltage for 15 minutes, and left for 30 minutes to obtain a stable state. The calculation of D_{Na+} is based on the formula:

$$D_{Na+} = \frac{4}{\pi}\left(\frac{mVm}{MA}\right)^2\left(\frac{\Delta E_s}{\Delta E_\tau}\right)^2 \quad \text{(S1.2)}$$

Among them, the ionic diffusion coefficient ($cm^2\ s^{-1}$), the mass of the electrode active substance (g), the molar molecular weight ($g\ mol^{-1}$), the molar volume of the cathode material ($cm^3\ mol^{-1}$), the area of the electrode (cm^2), the voltage change of the electrode during A charge/discharge time (V) and the voltage difference between the two transients before and after charge/discharge (V) can be represented by D_{Na+}, m, M, Vm, A, ΔE_τ, and ΔE_s, respectively.

Table S1 Comparison of half cell electrochemical performance with recent literature results.

Samples	Rate	Cycle	First Capacity	Final Capacity	Retention	Ref
NVPF@5% rGO	5	1000	83.2	78.2	94	1
C-$NaVPO_4F$	1	400	94.5	84.7	94.5	2
$NaVPO_4F$@C-750℃	2	300	116.2	103.6	89.2	3
15-SC@NVPF	0.5	1000	104	100.8	97	4
NVPF/C/CNT10%	5	1000	107.7	83.9	77	This work

1. Zhao, C. Guo, J. Gu, Z. Zhao, X. Li, W. Yang, X. Liang, H. Wu, X., Robust three-dimensional carbon conductive network in a $NaVPO_4F$ cathode used for superior high-rate and ultralong-lifespan sodium-ion full batteries. *Journal of Materials Chemistry A* **2020**, 8, 17454-17462.

2. Bin, D. Wang, Y. Tamirat, A. G. Zhu, P. Yang, B. Wang, J. Huang, J. Xia, Y., Stable High-Voltage Aqueous Zinc Battery Based on Carbon-Coated $NaVPO_4F$ Cathode. *ACS Sustainable Chemistry & Engineering* **2021**, 9, 3223-3231.

3. Zuo, Y. Yue, J. Ma, Z. Zuo, Z., Facile fabrication of carbon-encapsulated $NaVPO_4F$ nanocomposite as a high-rate and long-cycle life cathode material for sodium energy storage. *Journal of Physics and Chemistry of Solids* **2022**, 160, 110354.

4. Kumar, V. K. Ghosh, S. Biswas, S. Martha, S. K., Pitch-Derived Soft-Carbon-Wrapped $NaVPO_4F$ Composite as a Potential Cathode Material for Sodium-Ion Batteries. *ACS Applied Energy Materials* **2021**, 4, 4059-4069.